BIOMECHANICS OF THE INFERIOR GLENOHUMERAL LIGAMENT OF THE SHOULDER DURING THE SIMPLE TRANSLATION TEST

by

William Joseph Newman

A thesis submitted to the faculty of
The University of Utah
in partial fulfillment of the requirements for the degree of

Master of Science

Department of Bioengineering

The University of Utah

December 2003

ABSTRACT

The shoulder is one of the most complex and often injured joints in the human body. Injuries to the soft tissue restraints of the shoulder are frequently difficult to diagnose and treat effectively. The inferior glenohumeral ligament (IGHL) of the glenohumeral capsule is especially prone to injury, and differential diagnosis is difficult due to the multiple soft tissue structures that complement its function *in vivo*. The objective of this research was to examine the function of the IGHL during a clinical diagnostic procedure termed the "simple translation test" using the finite element method. A finite element (FE) model of the humerus, scapula, humeral head cartilage and IGHL was constructed from a subject-specific CT dataset. A repeatable reference state for strain measurement was established by using compressed air to inflate the capsule to a pressure of 1 KPa. The CT dataset was acquired while the capsule was inflated, and the finite element model geometry was extracted to mimic this configuration. Starting from this reference state, experimentally measured 6-DOF kinematics were applied to the finite element model. At maximum anterior translation, first principal strains in the IGHL were highly inhomogeneous. In the AB-IGHL, strains of 0-19% were predicted over all three angles of external rotation. Strains of 0-31% were predicted in the axillary pouch of the IGHL. In the PB-IGHL, strains of 1-38% were predicted. The highest strains occurred during maximum external rotation at the insertion sites. In the sensitivity study, reduction of the IGHL modulus by one standard deviation generally increased strains in

the IGHL near the scapula and decreased strains near the humerus, with changes ranging from –56.8 to 12.7 %. Regional strain results point to a transfer of load from the scapular insertion site of the IGHL to the humeral insertion site with increasing external rotation, in the form of increasing strain near the humerus and decreasing strain near the scapula. This could be due to the observation that as the material properties of the cartilage and IGHL were varied, the extent and location of contact between the IGHL and cartilage changed. Using the techniques developed within this research project, an improved understanding of the role of the IGHL in anterior stability of the joint can be gained. This will lead to better rehabilitation protocols and improved surgical procedures.

TABLE OF CONTENTS

LIST OF FIGURES

ACKNOWLEDGMENTS

I would like to thank my advisor and mentor Dr. Jeffrey Weiss for his guidance and support during my thesis research. I would also like to thank my committee members, Drs. Richard Rabbitt and Richard Debski, for their insight and knowledgeable support. I would like to acknowledge the assistance of Rich Debski and Susan Moore in the collection of kinematic data and experimental information contained within this thesis. Finally, I would especially like to thank my mother, L. Patricia Newman, for her support and encouragement, without which this work could not have been completed.

Financial support from Whitaker Grant #RG-99-0376 and NIH Grant #AR47369 is gratefully acknowledged.

CHAPTER 1

INTRODUCTION

Motivation

The glenohumeral joint is one of the most complex and frequently injured joints in the human body. It has the largest range of motion of any joint, which also makes it one of the most unstable and easily dislocated joints in the body. Glenohumeral stability is maintained through a complex combination of bony contact and soft tissue restraints that include the joint capsule, ligaments, labrum and muscles [1]. However, the role of the ligamentous capsule in providing glenohumeral stability has continued to be a source of controversy.

In general, there are three causes of shoulder instability. The shoulder can become unstable after acute injury. Repeated trauma is another main cause. This is common in athletes such as throwers and swimmers who use multiple repeated movements that put significant stresses on the glenohumeral capsular ligaments (Fig. 1.1). Finally, inherited defects of the connective tissue can cause shoulder instability. Detachment of the inferior glenohumeral ligament (IGHL) from the anterior glenoid and labrum, defined as a Bankart Lesion [2], as well as capsular stretching are frequent injuries for which initial and differential diagnosis are often difficult. Computational analyses such as the finite element (FE) method can be used to examine the function of

Figure 1.1. Extreme loads placed on the shoulder during skiing or repetitive motions such as pitching can lead to injury.

joints, allowing for the study of the effects of surgery, prediction of conditions that may lead to injury, and as an educational tool both for clinicians and patients [3-7]. The objective of this study was to construct FE models of the entire IGHL including the anterior band (AB), posterior band (PB) and axillary pouch, subject the models to applied kinematics representing a clinical test for anterior instability, and predict the strains in the IGHL and reaction forces due to contact under the prescribed motions.

Summary of Chapters

Chapter 2 describes the anatomy, structure and function of the glenohumeral joint, reviews existing knowledge and states the significance, objectives and hypotheses of this study. Chapter 3 describes the experimental methodology. Results of this study are presented in Chapter 4. Chapter 5 provides a discussion of the results, the strengths and limitations of this study, states the conclusions and establishes some guidelines for future work.

CHAPTER 2

BACKGROUND

Anatomy and Function of the Glenohumeral Capsule

The glenohumeral joint is made up of the humerus, scapula, cartilage, rotator cuff muscles and the ligamentous tissue of the capsule. The capsule is composed of a variably thick layer of tissue with discrete thickenings that constitute the glenohumeral ligaments, and includes the superior glenohumeral ligament (SGHL), middle glenohumeral ligament (MGHL) and the IGHL (Fig. 2.1) [8, 9].

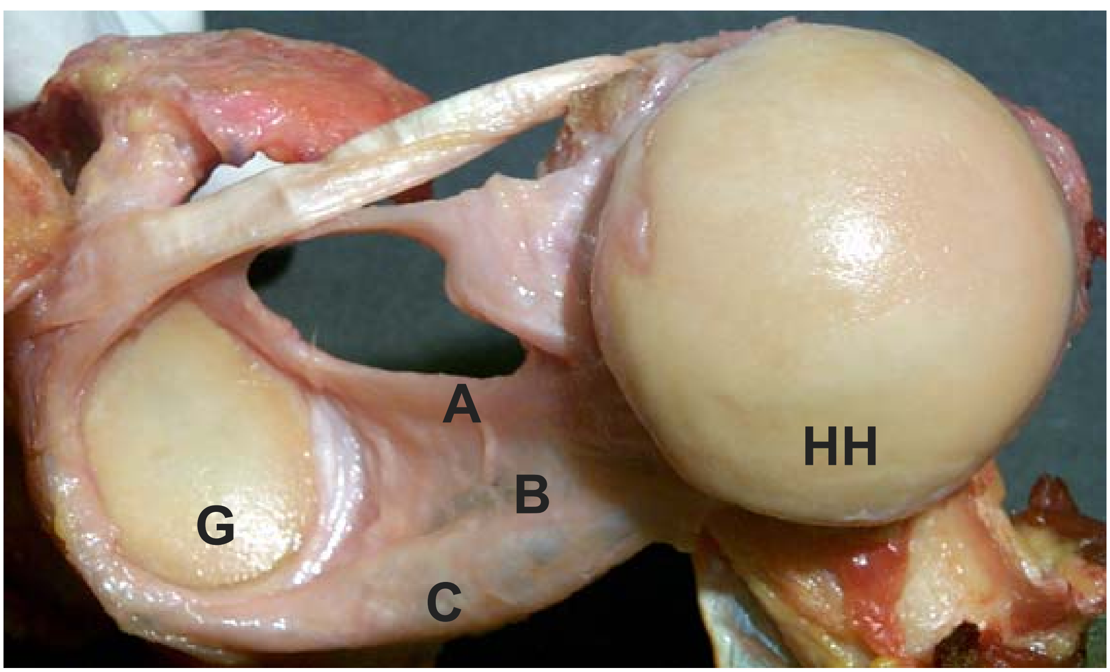

Figure 2.1. Lateral view of a disarticulated glenohumeral joint, showing the glenoid (G), humeral head (HH), PB-IGHL (A), axillary pouch (B) and AB-IGHL (C).

Different regions of the capsule have been shown to tighten at various extreme positions of glenohumeral motion. In this research, the joint position of primary focus was the humerus at 60 degrees of abduction, which is the position for the simulated clinical exam. It has been shown that the anterior portion of the capsule becomes the dominant restraint as abduction is increased with external rotation [10].

Existing Knowledge

Previous experimental studies have analyzed the strain in the IGHL under a range of applied loading conditions. Stefko et al. presented a study detailing IGHL stretching at glenohumeral failure through the apprehension position, citing the glenoid as the common site of failure for the AB-IGHL [11]. McMahon et al. examined the glenoid insertion site and quantified midsubstance irrecoverable elongation under tensile testing with the shoulder in abduction and external rotation [12]. Most specimens (64%) failed at the glenoid insertion site, and elongation of the ligament contributed to anterior instability. Bigliani et al. performed a landmark study that examined the tensile properties of the entire IGHL [13].

Malicky et al. performed a stereoradiogrammetric study of total strain fields of the antero-inferior shoulder capsule under subluxation [14]. This study determined that maximum principal strains were highly variable over the IGHL, with high strains occurring on the glenoid side of the ligament and unexpectedly discovered additional high strains at the humeral insertion site as well. This model also included the first measurement of a two-dimensional strain field of capsuloligamentous tissue. O'Connell et al. performed a study to investigate the contribution of the glenohumeral ligaments to anterior instability of the intact glenohumeral joint [15]. Hall-effect strain transducers were used to measure strain in the capsule while externally rotating and abducting the humerus of six specimens. Considerable variation in the strain were found; however, the anterosuperior band of the IGHL was a significant contributor to anterior stability of the shoulder.

Brenneke et al. examined the strain of capsular structures of the glenohumeral joint during laxity exams commonly used in orthopedic examinations using mercury strain gauges and an electromagnetic tracking device to record kinematics [16]. With the humerus in abduction and external rotation, the anterior middle, anterior-inferior and posterior middle ligaments became the primary restraints at the shoulder. Finally, in a study performed by Moore et al., bi-directional mechanical properties of the axillary pouch were examined through tensile testing [17]. This group found that properties of the pouch in the transverse direction were not significantly different from those measured in the longitudinal direction, which suggested that the axillary pouch functions to stabilize the joint in more than just the medial-to-lateral direction as previously assumed.

Arthroscopic examinations have confirmed that there is large variability in the size and appearance of the glenohumeral ligaments [18-20]. Voluminous studies have examined the structural and mechanical properties of glenohumeral ligaments, but only in uniaxial tension [12, 13, 21-24] [11, 25]. These studies are comprehensive when it comes to describing the structural and mechanical characteristics of the IGHL; however, there is a lack of any constitutive modeling to assist in predicting and diagnosing injury via analytical or computational methods.

Numerical methods developed in the field of computational mechanics offer a viable alternative to experimental studies. These approaches can be applied to better understand the mechanism of shoulder instability and to evaluate surgical techniques for repair of shoulder lesions. For example, Luo et al. [26] developed a simplified, two-dimensional finite element model of the supraspinatus tendon and used the model to predict the mechanism of rotator cuff injuries. The results of this study suggested additional tear mechanisms of the rotator cuff that were unaccounted for by traditional mechanical models. Novotny et al. [27] developed an anatomical model of the human GH joint to predict GH kinematics and investigate the mechanics of GH joint stabilization. While this research contributed to the understanding of how the individual bands of the IGHL act to avoid shoulder instability, the model did not use anatomical data to construct the bony surfaces or ligaments. The structural properties of the ligaments were described in terms of the stiffness and initial length. This approach does not allow for prediction of the multiaxial behavior of the capsule under various loading conditions.

More complex, finite element models of the shoulder mechanism have also been developed. Van der Helm [28] described a method for developing a three-dimensional musculoskeletal model of the shoulder mechanism. The inputs into the model included the geometry and relative locations of the bones, joints, ligaments, and muscles surrounding the shoulder complex, whereas the output variables included muscle forces. Muscles were represented by active uniaxial elements and the ligaments were represented by passive uniaxial elements. The ligament line of action was defined by a line connecting the centroids of the origin and insertion. EMG data were used to validate the predicted muscle forces in a qualitative sense and the results provided insight into the function of morphological structures of the shoulder [29]. While this model is beneficial for describing contributions from individual muscles, it was limited in its ability to describe internal ligament stresses under various loading conditions.

Debski et al. used an analytical approach to determine the forces in the GH ligaments during prescribed joint motions [30]. The bones were modeled as a set of rigid body segments connected by joints and the GH ligaments were modeled as a finite series of linear segments. The model predicted that during anterior loading without any abduction, the superior glenohumeral ligament carried the highest force at 71 N. However, during anterior loading and 90 degrees of abduction, the model predicted that the AB-IGHL carried the highest force at 45 N. These results were in agreement with previous experimental studies. It was suggested that this approach could be used to predict the forces in the GH ligaments during more complex joint motion, as well as to assist surgeons during shoulder repair procedures. This model did not include consistent anatomic geometry of the shoulder complex nor did it account for the fiber properties of the ligament. Although the loads within the GH ligaments were calculated, the model was limited in its ability to determine the stress-strain distribution within the ligaments. Additionally, it was suggested that some of the specific assumptions used in the model resulted in inconsistencies in the analytical results. In particular, the model did not account for deformations at the insertion site of the GH ligaments during loading of the GH capsule. This simplification may have a pronounced effect on predictions of deformation for the AB-IGHL and the PB-IGHL. Furthermore, the reference length and load-elongation properties of the GH ligaments may not have been ideal for the joint geometry used in the model.

Although these experimental and computational studies have elucidated some aspects of the mechanics of individual ligaments of the shoulder complex, there is still controversy as to the mechanism of shoulder instability. As evidenced by these studies, computational models of the capsule and ligaments at the glenohumeral joint have not considered the true continuous nature of the capsule.

Collagen Fiber Alignment

Collagen fiber orientation is an important determinant of ligament structural and mechanical properties. Generally, as fiber alignment increases with the direction of load application, the more the ligament is able to bear load without failure. Knowledge of collagen fiber alignment can assist in selecting the most appropriate constitutive model for use during FE analysis. The orientation of the collagen fibers within each of the three regions of the IGHL has been qualitatively examined in two studies utilizing polarized light microscopy [31] [9].

In another study, Debski et al. demonstrated that the collagen fiber alignment throughout the thickness of the axillary pouch was random [32]. A small angle light scattering device (SALS) [33, 34] was used to observe fiber direction in eight specimens. This device passes a 4mW HeNe continuous unpolarized wave laser through the tissue. The laser light scatters according to the internal fiber structure within the light beam envelope. The spatial intensity distribution of the resulting scattered light represents the sum of all structural information within the light beam envelope. When scattered light intensity is plotted against the rotation angle at a constant radius from the optic axis, it represents the angular fiber orientation. Due to the apparent lack of collagen fiber alignment, the axillary pouch did not appear to have the morphological characteristics of a traditional ligament - that is, a high degree of collagen fiber alignment with respect to its longitudinal axis. As a result, it was determined that a globally isotropic material model may be appropriate for representing the material behavior of the glenohumeral capsule.

Significance

Previous models have measured or described the capsule as consisting of individual uniaxial structures, neglecting the continuous nature of the capsule. By investigating the strain fields throughout the capsule, the current knowledge of the functional role of the capsular regions can be enhanced. Previous models have not been based on specimen-specific anatomical data. This may have led to errors in predictions due to the morphological differences between individual joints and ligaments. These errors can be corrected by basing computational models on specimen-specific geometry.

The process used in this research is a critical step to enhance the current understanding of how stress and strain fields in the IGHL correspond to joint position, and forms one block of the foundation for a long-term research plan that will examine the cause of glenohumeral pathology and restoration of normal joint function following surgical repair and rehabilitation.

Objectives and Hypotheses

The primary objective of this research was to develop methods for subject-specific modeling of the ligamentous structures of the glenohumeral joint and to determine the regional IGHL strain distribution during a simulated clinical exam using the finite element (FE) method. A second objective of this study was to determine the sensitivity of the model to changes in material coefficients of the humeral cartilage and IGHL. Based on previous studies [12] [14], it was hypothesized that strains and stresses would increase near the insertion sites and decrease at the midsubstance of the IGHL during application of the kinematics of the simple translation test. This testing of this hypothesis will demonstrate the efficacy of using finite element analysis as a method to study joint biomechanics.

CHAPTER 3

METHODS

Overview

Experimental and computational methods were combined to develop the FE models used in this study (Fig. 3.1): First, the kinematics of an intact shoulder joint were measured experimentally during the “simple translation test”. After experimental testing, a CT scan of the specimen was acquired. Surface models of relevant geometries were generated, and a FE mesh of the joint was constructed. Material properties acquired from previous studies were used as input to the model. Outputs from the finite element model

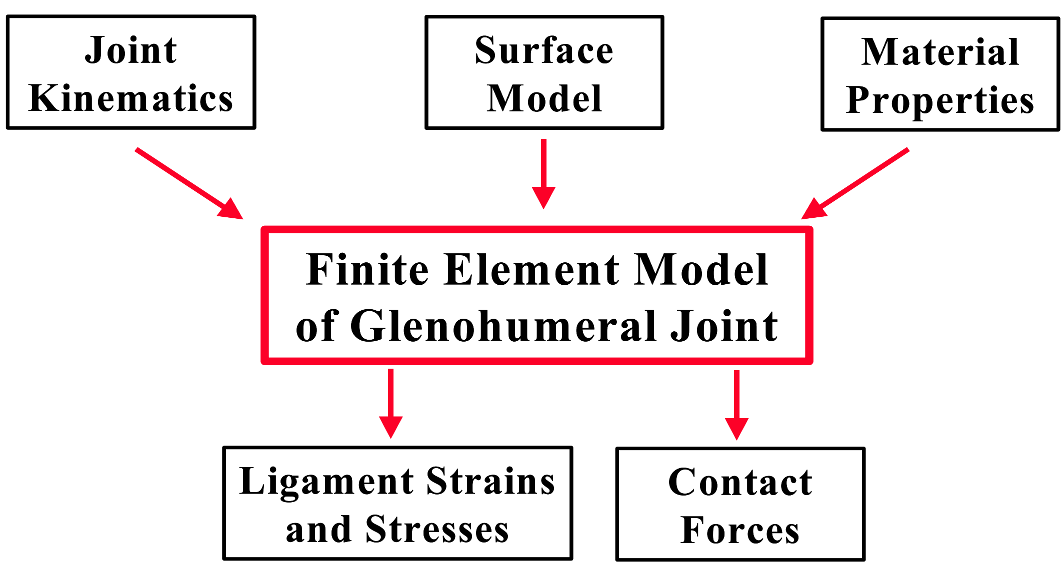

Figure 3.1. Flowchart demonstrating the experimental process.

included predicted strains, stresses and total contact force between the IGHL and humeral head cartilage.

Experimental Measurement of Shoulder Kinematics

An intact shoulder joint (F, 64 y.o.) was dissected, leaving the mid-humerus, scapula, rotator cuff muscles and capsule (vented at the rotator interval) intact. Plexiglas blocks were adhered to the scapula and humerus to allow the definition of local coordinate systems for co-registration of kinematic and CT datasets [35]. The scapula and humerus were then fixed in epoxy putty.

The scapula was mounted vertically in a Plexiglas fixture and 13.4 N was applied to each of the rotator cuff muscles [36] (Fig. 3.2). Using a magnetic tracking device (Flock of Birds, Ascension Technologies, Inc.), the Plexiglas blocks were digitized and

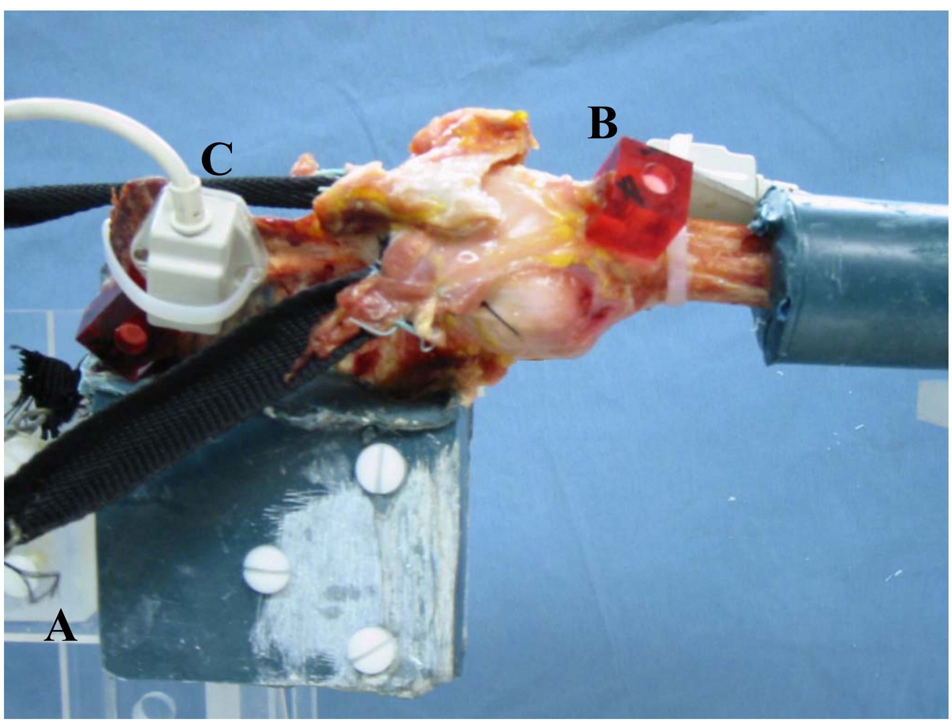

Figure 3.2. Cadaveric shoulder mounted in (A) Plexiglas jig, with (B) registration blocks attached and the (C) electromagnetic tracking sensors.

local coordinate systems were established. The soft tissues were preconditioned to minimize the effect of viscoelasticity by cycling the joint between the neutral position and maximum anterior and posterior translation. Next, the clinician translated the humeral head to its limit in the anterior and posterior direction at 0º, 30º, and 60º of external rotation (ER) and 60° of abduction while the joint kinematics were continuously recorded.

The method described by Simo and Qu-Voc was used to convert the transformation matrices from the tracking system into quaternions [37]. The commercially available program Matlab 6.1 (The Mathworks, Inc.) was used to execute the algorithm (Appendix). The transformation matrix between the registration blocks was obtained from the tracking system for each time step:

$$T = \begin{bmatrix} R_{11} & R_{12} & R_{13} & t_1 \\ R_{21} & R_{22} & R_{23} & t_2 \\ R_{31} & R_{32} & R_{33} & t_3 \\ 0 & 0 & 0 & 1 \end{bmatrix}. \tag{3.1}$$

Here R_{ij} are the components of the orthogonal 3x3 rotation matrix and the t_i are the components of the translation vector between the coordinate systems. Next, Spurrier's algorithm was used to derive the quaternions corresponding to each transformation matrix:

$$M := \max(\Lambda_{ii}; \Lambda_{11}, \Lambda_{22}, \Lambda_{33}) \tag{3.2}$$

If $M = \Lambda_{ii}$, then:

$$q_0 = \frac{1}{2}\sqrt{1+\Lambda_{ii}}, \tag{3.3}$$

$$q_i = (\Lambda_{kj} - \Lambda_{jk}) / 4q_0 \text{ for } i = 1,2,3 \tag{3.4}$$

Else:

Let i be such that $M = \Lambda_{(ii)}$,

$$q_i = \left[\frac{1}{2}\Lambda_{(ii)} + \frac{1}{4}(1 - \mathrm{Tr}(\mathbf{\Lambda})) \right]^{1/2}, \tag{3.5}$$

$$q_0 = (\Lambda_{kj} - \Lambda_{jk}) / 4q_i, \tag{3.6}$$

$$q_l = (\Lambda_{li} - \Lambda_{il}) / 4q_i \text{ for } l = j, k, \tag{3.7}$$

where (i, j, k) is a cyclic permutation of (1,2,3). Here, M is a defined variable, Λ_{ii} is a component of the transformation matrix and q is a quaternion.

Then, the incremental translations and rotations extracted from the quaternions using a method outlined by Maker [38]:

$$\alpha = (q_1^2 + q_2^2 + q_3^2)^{1/2}, \tag{3.8}$$

$$\beta = \begin{cases} \dfrac{2}{\alpha}\sin^{-1}\alpha, & \alpha \geq 10^{-6} \\ 0 \quad , & \alpha < 10^{-6} \end{cases}.$$

Here, α is calculated from the quaternions, β is calculated from α and the incremental rotations (r_x, r_y and r_z) are calculated from both beta and the quaternions. The incremental translations (*dx*, *dy* and *dz*) come directly from the transformation matrix. Finally, the last step was to subtract the values of incremental rotations and translations between each successive time step during the experiment. The data were entered as "load curves" in the finite element code to drive the relative motion of the bones.

CT Scan, Surface Reconstruction and Mesh Generation

The insertion sites of the IGHL on the humerus and scapula were marked arthroscopically with copper wires, and rubber tubes were used to mark boundaries of the anterior band (AB-IGHL), posterior band (PB-IGHL) and axillary pouch. Nylon beads were placed on the surface of the axillary pouch (Fig.3.3). The rubber tubes and nylon beads facilitated clear visualization of the regions and geometry of the IGHL in the CT

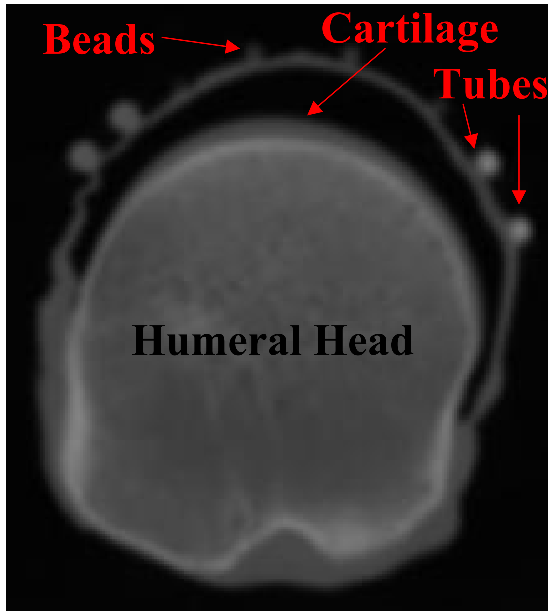

Figure 3.3. CT scan showing the rubber tubes, nylon beads and HH cartilage.

images for surface reconstruction. Compressed air (1 KPa) was injected into the joint space in order to define a reference position for strain measurement that minimized wrinkles and folds in the capsule [39].

Once the reference configuration was established (60° abduction, 45° external rotation, 0° flexion), a volumetric CT dataset was acquired (slice thickness = 1 mm, FOV = 150 mm, in-plane resolution = 512x512). Relevant structures in the dataset such as the humerus, scapula, humeral head cartilage, IGHL and rubber tubes were hand-digitized from the CT images to produce spline contours (Fig. 3.4). The spline contours corresponding to all of the CT images were stacked up and laced together to produce polygonal surfaces using the public-domain NUAGES software [40] (Fig. 3.5). Contours of the rubber tubes and insertion sites were used to guide construction of the FE meshes of the IGHL (Fig. 3.5).

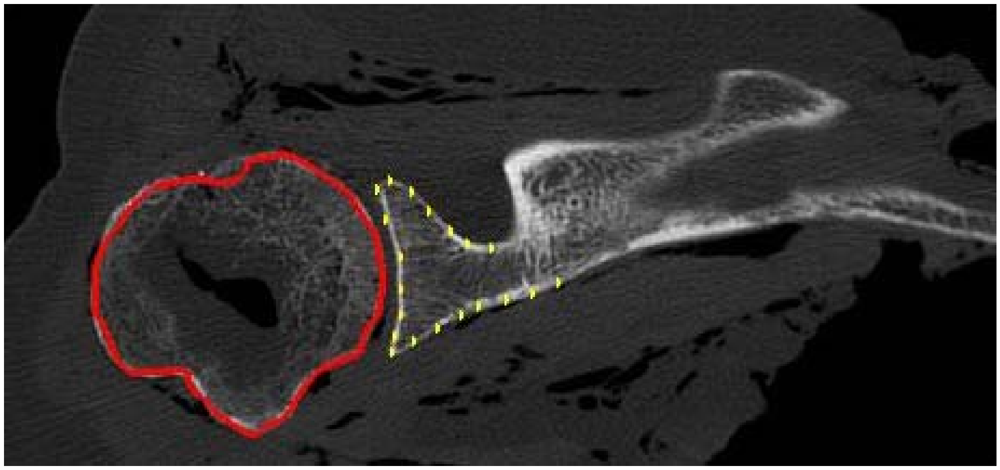

Figure 3.4. CT slice showing hand-digitized spline contours.

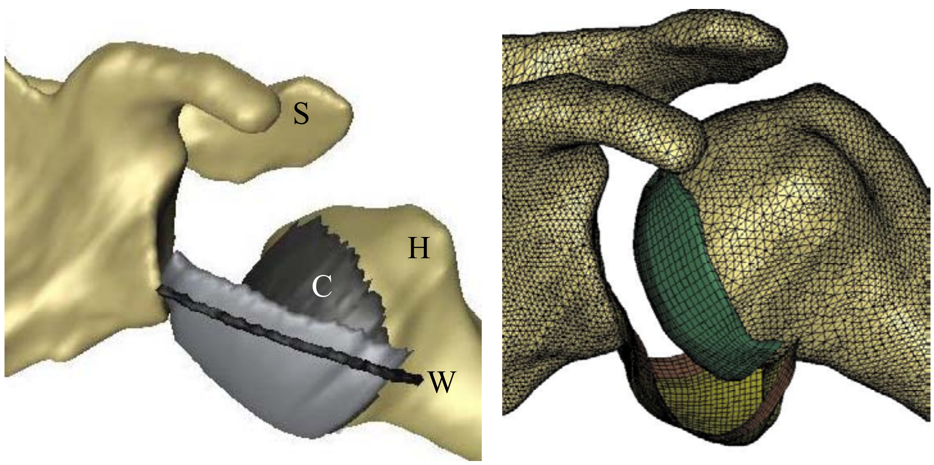

Figure 3.5. Left – Surfaces reconstructed from CT data showing humerus (H), scapula (S), humeral head cartilage (C), IGHL and rubber wire (W). Right – FE mesh showing the humerus, scapula, humeral head cartilage and IGHL.

The surface definitions were imported into a finite element preprocessor (TrueGrid, XYZ Scientific, Livermore, CA). Triangular surfaces representing the bones were converted directly to rigid body shell meshes [38]. The surfaces of the IGHL, cartilage and rubber tubes were used to generate the finite element meshes.

Material Properties

The humeral head cartilage was modeled as an isotropic Mooney-Rivlin material [41], using 8-node hexahedral elements to discretize the geometry. Material coefficients (C_1 and C_2) were based on data in the literature (C_1=4.147 MPA and C_2=0.414 MPa) [42]. The modulus and poisson's ratio of the IGHL (E=9.1 MPa, ν=0.4) were based on values used in a previous study [17]. Shell elements were used to represent the IGHL [43]. The shell elements provide more realistic (i.e., softer) behavior during bending in comparison to solid hexahedral elements [44].

Boundary Conditions

The entire FE model was transformed so that the global coordinate system was aligned with the coordinate system of the scapular registration block [35]. The rigid body motion of the humerus with respect to the scapula was described by incremental translations and rotations referenced to the coordinate systems of the registration blocks as described previously. The finite element mesh of the AB-IGHL was attached to the scapula and humerus by specifying rigid node sets at the proximal and distal ends of the mesh. These node sets were prescribed to move with the corresponding bones. A similar approach was used to attach the hexahedral cartilage FE mesh to the humeral head. Frictionless contact surfaces were defined between the IGHL and humeral head cartilage. Contact was enforced using the penalty method [41].

Finite Element Analysis

The implicitly integrated FE code NIKE3D was used for all analyses [41]. An incremental-iterative solution strategy was employed, with iterations based on a quasi-Newton method [45] and convergence based on the L_2 displacement and energy norms [38]. Thus, increments in the experimentally measured kinematics were applied to the model over quasi-time, and the timestep size was adjusted using an automatic procedure. Computations were carried out on a two-processor Compaq DS20E with 4 GB of core memory. The average run time was 2.5 hours for each analysis .

Postprocessing

Results from the finite element analysis were imported into the LSPOST post-processor (Livermore Software Technology Corporation, Livermore, CA). Graphical results such as fringe plots of regional first principal strain and stresses were viewed and regional strains were extracted. Regions of contact were also quantified based on the "penetration distance" predicted by the contact algorithm. Contact forces and rigid body reaction forces were obtained directly from the output of NIKE3D, and the magnitudes of these forces were calculated.

Regional Strains, Stresses and Contact Force

To facilitate analysis of the data and comparison between different loading conditions, 12 anatomical locations were defined on the IGHL (Fig. 3.6). Locations 1, 4, 7 and 10 corresponded to the AB-IGHL. Locations 2, 5, 8 and 11 corresponded to the axillary pouch, and locations 3, 6, 9 and 12 corresponded to the PB-IGHL. These

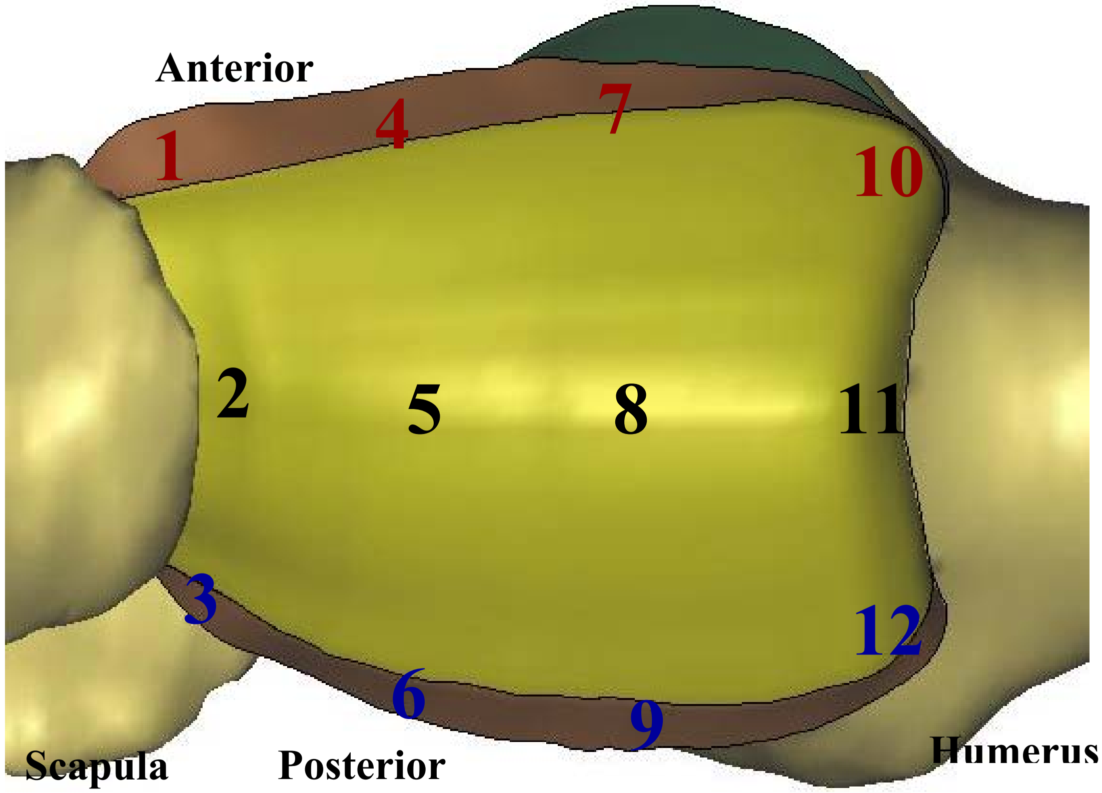

Figure 3.6. Locations of measurement (inferior view). Red locations represent the AB-IGHL, black locations represent the axillary pouch and blue locations represent the PB-IGHL.

locations were chosen to provide a representative sampling of each major component of the IGHL. The predicted measurements were compared to values in the literature at these locations. The stress distribution on the inferior surface of the IGHL was plotted at each angle of external rotation using LSPOST.

Sensitivity Studies

Sensitivity studies were performed to determine the effect of changes in material properties on predicted strains. Strains were measured at selected regions of the IGHL at 60 degrees of external rotation to serve as baseline values for the parameter study (Fig.

3.6). Locations of measurement included the scapular insertion site (regions 1, 2 and 3), midsubstance (region 5) and humeral insertion site (regions 10, 11 and 12). These locations were chosen for their importance in stretching and failure of the IGHL [12]. Material coefficients of the humeral head cartilage (C_1 and C_2) were varied by a single order of magnitude, from 4.137 and .4137 respectively. The modulus for the IGHL was varied by one standard deviation (±6.4) from 9.1 MPa (Moore 2002).

CHAPTER 4

RESULTS

Regional Strains

Regional strains in the AB-IGHL, PB-IGHL and axillary pouch were determined as a function of location along the ligament. The predicted strains were calculated and tabulated for each region and angle of external rotation (Tables 4.1, 4.2 and 4.3). The locations of measurement were based on regions described in Figure 3.6 as shown in the section above. Strains in each region were then graphed for the AB, PB and axillary pouch as a function of location along the IGHL, starting at the scapular insertion site and ending at the humeral insertion site (Figs. 4.1, 4.2 and 4.3).

At maximum anterior translation, first principal strains in the IGHL were inhomogeneous over its length. In the AB-IGHL (regions 1, 4, 7 and 10), strains of 0-19% were predicted over all three angles of external rotation. Strains of 0-31% were predicted in the axillary pouch of the IGHL (regions 2, 5, 8 and 11). In the PB-IGHL, strains of 1-38% were predicted (regions 3, 6, 9 and 12). Strains at the scapular insertion site (regions 1, 2 and 3) ranged from 4-39%. Strains in the midsubstance of the IGHL (regions 4, 5, 6, 7, 8 and 9) ranged from 0-11%. Predicted strains at the humeral insertion site (regions 10, 11 and 12) ranged from 1-28%.

Table 4.1. Regional first principal strains at 0 degrees of external rotation.

	Scapula	Midsubstance	Midsubstance	Humerus
AB-IGHL	.0653	.0001	.0307	.1532
AP	.0403	.0320	0	.0009
PB-IGHL	.3833	.0117	.0343	.0363

Table 4.2. Regional first principal strains at 30 degrees of external rotation.

	Scapula	Midsubstance	Midsubstance	Humerus
AB-IGHL	.0428	.0200	0	.0802
AP	.2283	.1024	.0273	.2001
PB-IGHL	.1339	.0359	.0218	.0345

Table 4.3. Regional first principal strains at 60 degrees of external rotation.

	Scapula	Midsubstance	Midsubstance	Humerus
AB-IGHL	.0393	.0057	.0004	.1956
AP	.3080	.1118	.0049	.2831
PB-IGHL	.0902	.0623	.0009	.2215

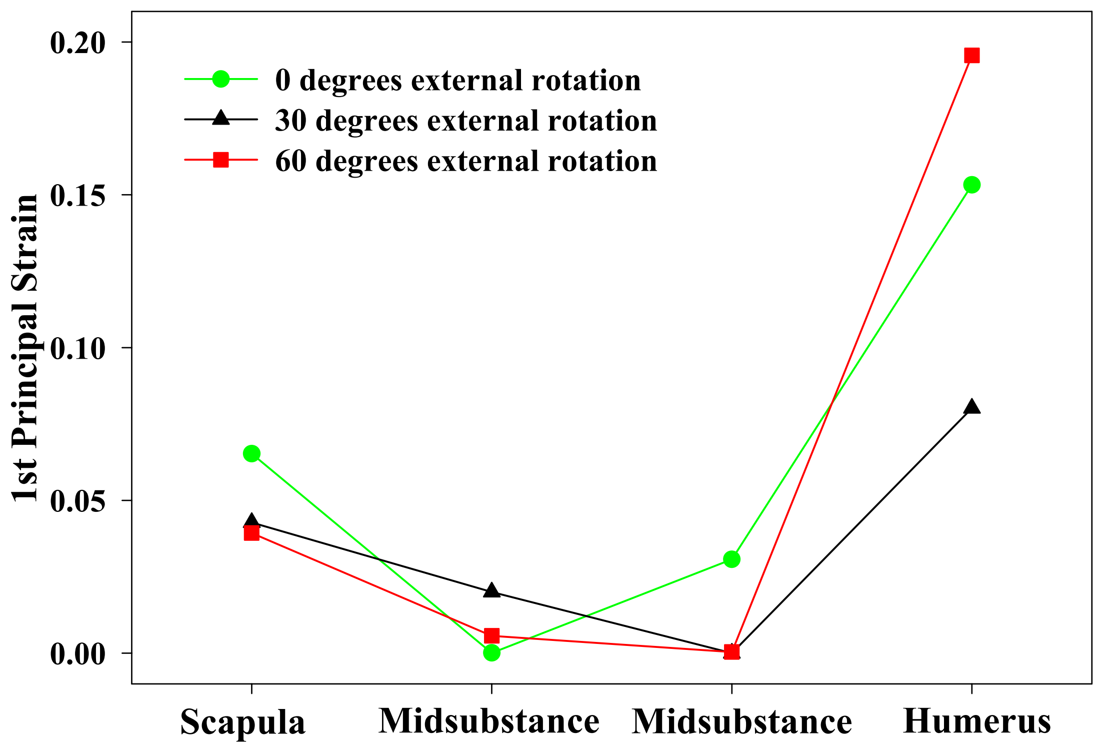

Figure 4.1. Regional first principal strains in the AB-IGHL.

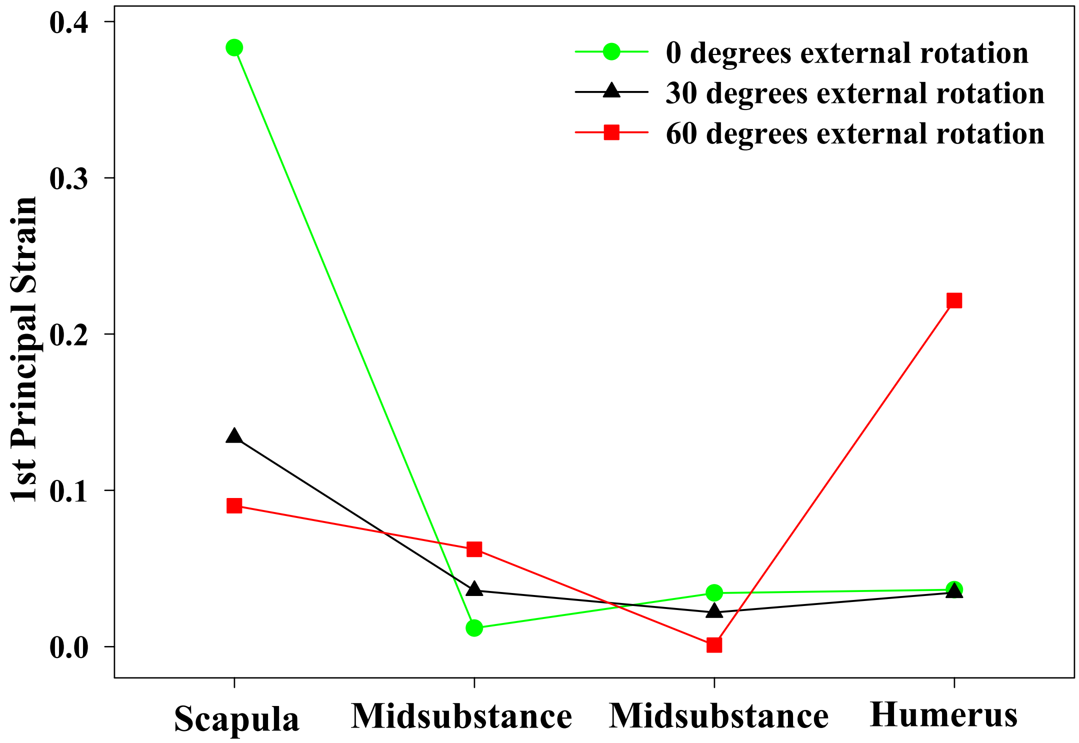

Figure 4.2. Regional first principal strains in the PB-IGHL.

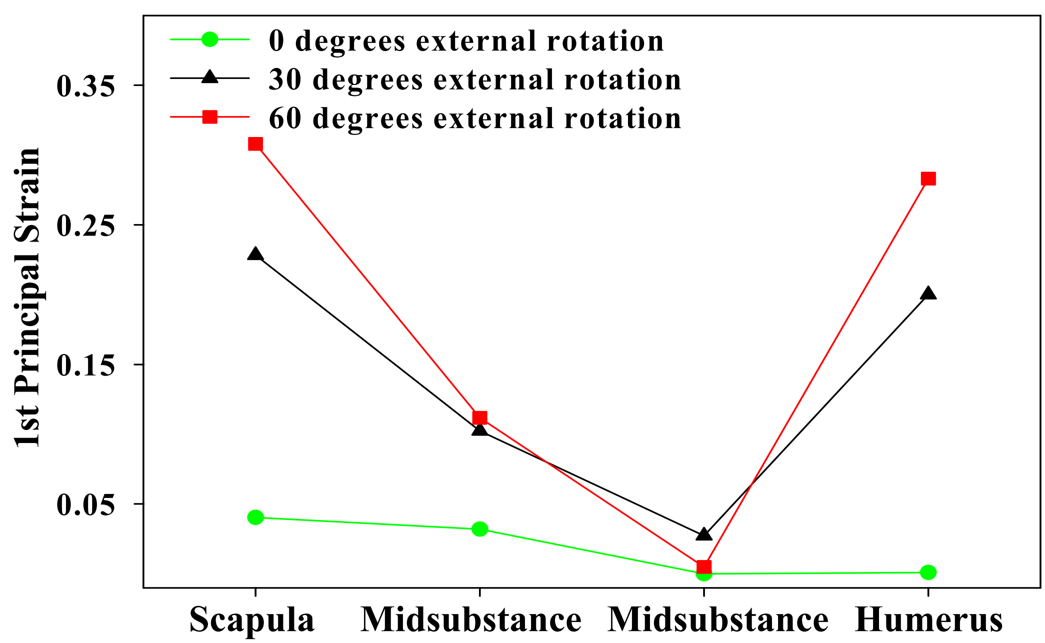

Figure 4.3. Regional first principal strains in the axillary pouch.

FE analysis was performed at all three external rotation angles. Fringe plots were generated at maximum anterior translation for each angle of external rotation to demonstrate the regions of highest predicted strain in the IGHL (Fig. 4.4). An inferior view of the strain distribution at 60 degrees of external rotation was also generated to serve as a reference figure (Fig 4.5). It shows the regions of high and low predicted strains during maximum anterior translation.

Stress Distribution and Contact Force

Results for the distribution of first principal stress on the interior surface of the IGHL show maximums of approximately 10.2 MPa at the scapular and humeral insertion sites at 60 degrees of external rotation and maximum anterior translation (Fig. 4.6). A measure of penetration distance (mm) of the shell element IGHL into the hex element humeral head cartilage was used to estimate the area of contact between the IGHL and humeral head cartilage (Fig. 4.7). Increasing area of contact was observed as the angle of external rotation increased. Total contact force, which is the magnitude of summed vectors describing the amount of contact between the IGHL and humeral head cartilage, and reaction force at the humeral insertion site, which is force measured at the humeral center of mass, for each angle of external rotation were calculated and graphed (Fig. 4.8). Maximums of 34 N for total contact force and 33 N for reaction force were found at 60 degrees of external rotation. Contact force and reaction force increased with increasing angle of external rotation.

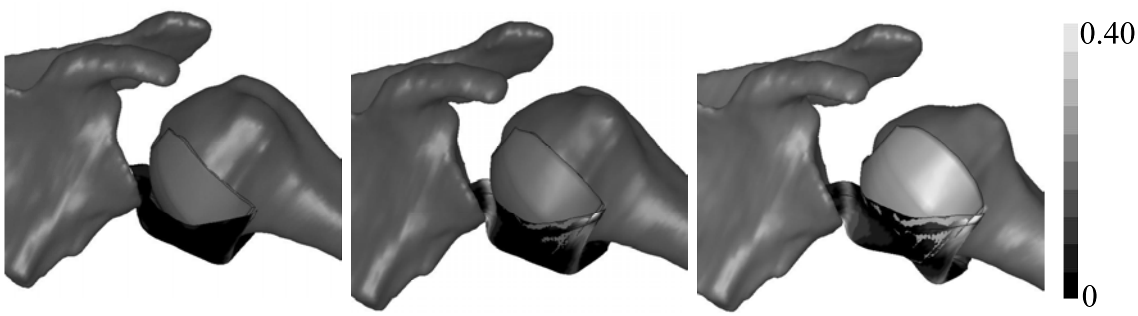

Figure 4.4. Fringe plot of the first principal strain at (A) 0 degrees, (B) 30 degrees and (C) 60 degrees of external rotation at maximum anterior translation. Strain and penetration of the IGHL increase with increasing ER.

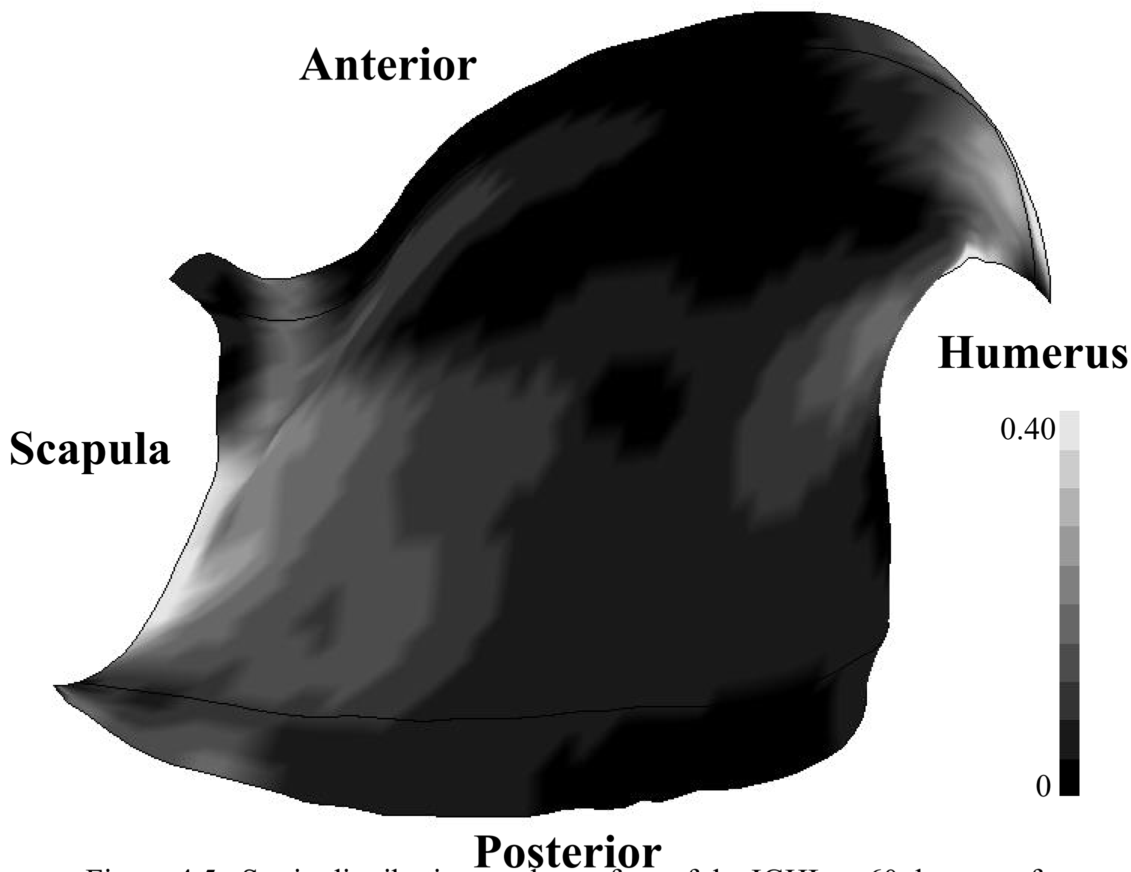

Figure 4.5. Strain distribution on the surface of the IGHL at 60 degrees of external rotation (inferior view). Highest strains occur near the anterior humeral insertion site and the posterior scapular insertion site.

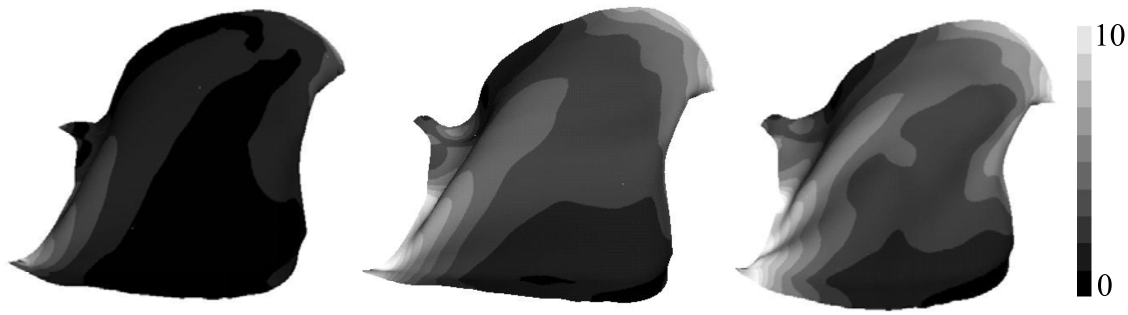

Figure 4.6. Distribution of first principal stress (MPa) at (A) 0 degrees, (B) 30 degrees and (C) 60 degrees of external rotation (inferior view). Stress increases with increasing angle of ER at the insertion sites and along areas of bending in the IGHL.

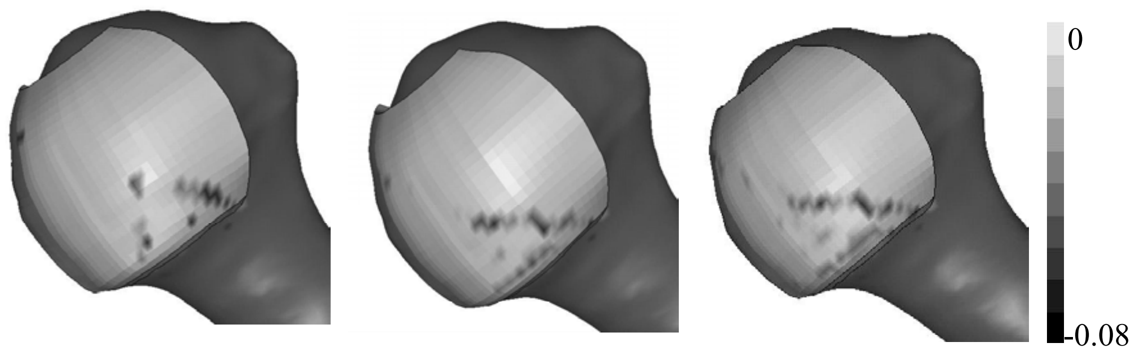

Figure 4.7. Penetration distance (mm) of the IGHL into the humeral head cartilage at (A) 0 degrees, (B) 30 degrees and (C) 60 degrees of external rotation. Increasing contact between the IGHL and cartilage is observed with increasing angle of ER.

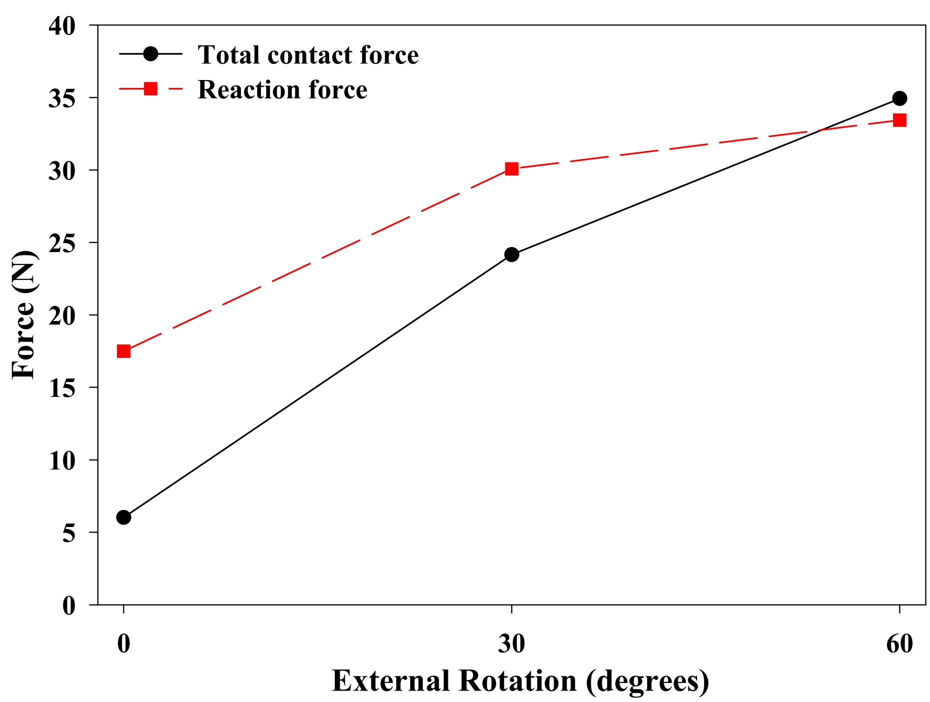

Figure 4.8. Contact force and reaction force at the humeral center of mass graphed as a function of external rotation angle. Both measures increase with increasing ER.

Sensitivity Studies

For the sensitivity studies, results the predicted regional strains at 60 degrees of external rotation and maximum anterior translation were used as a baseline for comparison (Table 4.4). When material properties of the cartilage were increased by an order of magnitude, strains generally increased near the scapular insertion site (regions 1, 2 and 3) and decreased near the humeral insertion site (regions 10, 11 and 12), falling anywhere from –57.6 to 17.7 % change from the measured baseline (Fig. 4.9). When the material properties of the cartilage were decreased by an order of magnitude, the strains decreased by –57.2 and 29.7 %. When the modulus of the IGHL was increased by one standard deviation, strains generally increased near the scapular insertion site and decreased near the humeral insertion site, ranging from –43.0 to 15.8 %. Reduction of the IGHL modulus by one standard deviation generally increased strains in the IGHL near the scapula and decreased strains near the humerus, with changes ranging from –56.8 to 12.7 %.

Contact forces were calculated for each model in the parameter study. When the modulus of the IGHL was increased and decreased, contact forces were 69.31 N and 12.03 N, respectively. When the cartilage coefficients were increased and decreased, contact forces were 47.21 N and 34.43 N, respectively.

Table 4.4. Values of strain at selected regions of the IGHL at maximum anterior translation and 60 degrees of external rotation.

Region	1	2	3	5	10	11	12
Strain(δ)	.0393	.3080	.0902	.1118	.1956	.2831	.2215

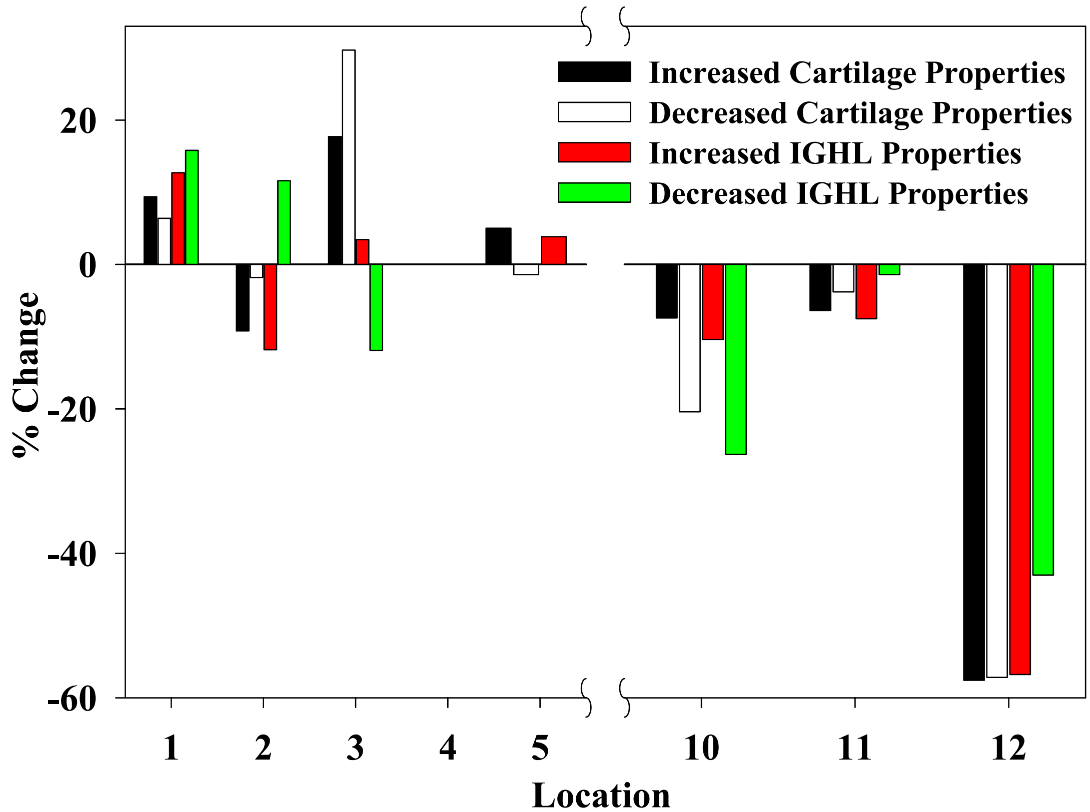

Figure 4.9. Bar graph showing percent change in measured strain as a function of location on the IGHL as the material properties of the cartilage and IGHL are varied.

CHAPTER 5

DISCUSSION

The objective of this research was to develop methods for subject-specific modeling of the capsuloligamentous structures of the glenohumeral joint and to determine the regional IGHL strain distribution during a simulated clinical exam using the FE method. A model of the IGHL was constructed and FE analysis of the simple translation test was performed.

The hypothesis was that strains observed for the IGHL would increase near the insertion sites and remain relatively constant through the midsubstance during kinematics of the simple translation test. In the AB-IGHL, predicted strains were generally uniform in the midsubstance and high at the scapular insertion site, while strains increased at the humeral insertion site at maximum external rotation (Fig. 4.1). In the PB-IGHL, predicted strains were relatively constant throughout, except at the scapular insertion site at 0 degrees of external rotation and at the humeral insertion site at maximum external rotation (Fig. 4.2) where strains also increased. In the midsubstance, strains were low through all angles of external rotation (Fig. 4.3). These results, combined with the fringe plots of surface stress (Fig. 4.6), show that the IGHL stretches significantly at the insertion sites and deforms in a pattern of mostly longitudinal folding at the midsubstance during abduction and external rotation, which supports the observation that the majority of IGHL injuries occur at the insertion sites during overhead sports such as swimming and tennis [24] [12].

It is important to note that strains in both the AB-IGHL and PB-IGHL dropped significantly at the scapular insertion site at 0 degrees of external rotation, and that strains in both the AB-IGHL and PB-IGHL increased significantly at the humeral insertion site at 60 degrees of external rotation. This points to a transfer of load from the IGHL to the humeral head as the IGHL wraps around the humeral head cartilage at maximum anterior translation and external rotation. This result is in agreement with an earlier study of the AB-IGHL [46], where results pointed to large degrees of wrapping and possible load transfer to the humeral head. This difference in results could be due to the fact that the previous study modeled just the AB-IGHL as a transversely isotropic hyperelastic material with the fibers running along the length of the ligament, whereas this study modeled the entire IGHL as nonlinear hypoelastic with random orientation of fibers.

The predicted magnitudes of strain and regions of maximum strain during the simulated simple translation test are in reasonable agreement with data of previous experimental studies that measured strain during tensile testing or functional loading experiments. In a study performed by Malicky et al. [14], maximum principal strains of the IGHL were shown to increase with increasing amount of subluxation, to a maximum of 31% strain near the scapular insertion site. In a study performed by Stefko et el. [11], strain at the midsubstance of the AB-IGHL at the time of capsular failure ranged from 3.68% to 10.68%. In another study by Bigliani et al. [13], tensile tests of the different regions of the IGHL yielded an average of 3.3 to 7.7 MPa at failure and 18.1% to 35.9% strain at failure. A study by Moore et al. [17] found that ultimate stress in the AB-IGHL ranged from 1.3 to 5.5 MPa, and ultimate strain reached 32% to 88%. Finally, in a tensile test study of the AB-IGHL by McMahon et al. [12], average stresses and strains at failure were found to be 7.3 to 9.7 MPa and 10% to 12.4%, respectively. In the present study, predicted values of maximum strain reached 19% and 38% in the AB and PB-IGHL, respectively, while maximum stresses reached 10.2 MPa. These results fall within the limits established by the literature mentioned above; however, the maximum predicted stress is somewhat high.

Differences between the results of the current study and the previous experimental results can be attributed to the loading conditions, strain measurement technique and the amount of capsule present. However, the data similarly suggest that the strain distribution varies throughout the AB-IGHL and the location of strain measurement is an important parameter.

Inferior surface stress distribution in the IGHL (Fig. 4.6) increased towards the insertion sites of the IGHL as external rotation increased. This demonstrates a transfer of load through portions of the IGHL as expected by the similar shift of regions of high strain. Highest stresses were observed where the IGHL shell element mesh inserted into the scapula and humerus at maximum external rotation and anterior translation. Contact area along the humeral head and contact force between the IGHL and humeral head cartilage also increased with external rotation (Fig. 4.7 and 4.8). This contributed to the increase in strain observed along the length of the AB-IGHL. Contact forces and rigid body reaction forces at the humeral center of mass were found to increase (Fig. 4.8) for each angle of external rotation. This is somewhat expected due to the fact that as contact area and magnitude increase between the IGHL and humeral head cartilage, the amount of total generated contact force increases as well.

The sensitivity study yielded surprising results. It was expected that as cartilage stiffness increased and IGHL modulus decreased, the overall strain observed in the IGHL would increase, due not only to the greater ability for the IGHL to stretch, but also to a decreased ability of the cartilage to deform. Conversely, as the cartilage properties decreased and the IGHL properties increased, the observed strain in the IGHL was expected to decline. Results demonstrated that this line of reasoning did not apply. Rather, a general increase in strain was observed near the scapular insertion site and a general decrease in strain was observed at the humeral insertion site as material properties were varied. The largest change in strains occurred at region 12, which is the posterior edge of the humeral insertion site. This location does not contact the cartilage. However, very little change in strain occurred at the midsubstance with changes in the modulus of the IGHL and the cartilage. This phenomenon could be due to the fact that as the material properties of the cartilage and IGHL are varied, the extent and location of contact between the IGHL and cartilage changes. This likely affects the predicted strain distribution in the IGHL. This finding emphasizes the need to acquire material properties of the IGHL and humeral head cartilage for each subject-specific specimen in future experiments, instead of relying on data found in the literature.

This issue can be further explained by examining the total contact forces between the cartilage and IGHL as the material properties were varied. Greater contact forces were observed when the IGHL and cartilage became stiffer. The general increase in strains predicted near the scapular insertion site, regardless of material properties, can now be explained by the fact that the majority of contact occurs toward the humeral insertion site of the IGHL. As a result, the IGHL increasingly stretches near the scapular insertion site. It is also possible that observed strains near the humeral insertion site generally decrease as a result of the large surface area involved during contact.

One of the limitations of this study is the fact that only a portion of the shoulder capsule was modeled. It is possible that load sharing between the IGHL and the rest of the capsule would alter the predictions of this study. Additionally, the rotator cuff tendons crossing the joint may alter the predicted strain distributions [47] [9]. This could affect the accuracy of the predictions obtained from the FE model. However, the method used in this study has been previously shown to be a reliable way to predict stresses and strains in the absence of muscles [48] [49].

The present model includes a larger portion of the capsule than any computational study done previously [27] [50] [28]. Furthermore, the present modeling approach utilizes experimentally measured kinematics to specify the relative motion of the bones during a simulated clinical exam under anesthesia. Thus, although alterations in joint motion due to the presence of additional muscles may change the predicted strains, the present approach provides an excellent representation of the kinematics that were measured experimentally.

This study modeled only a single subject-specific specimen. In finite element studies, it is normal to construct and analyze several individual models. Problems arise when relying on results from a single model due to the many boundary conditions and parameters that are adjusted during analysis, as well as anatomical variation in the geometry of individual joints. These problems can be reduced by using a larger sample size. As a result, the significance and reliability of the results could be greatly improved.

Cartilage of the glenoid and the labrum is very important to glenohumeral stability, and adds to the "ball-and-socket" properties that this joint exhibits; it also plays a role in the IGHL insertion site [51] [52]. These structures were not included in this model due to difficulty in differentiating the structures from the CT data; however, the IGHL does not come into contact with the glenoid or labrum during the simple translation test, so including the labrum and glenoid cartilage became irrelevant.

A final limitation is that no experimental data exist to validate this model. The best that can be done is to compare the predicted strains to those found in the literature; however, the reults from this model compare favorably to values found in the literature [12] [17] [14] [13] [11].

Several assumptions were made about the material behavior of the IGHL and cartilage of the humeral head. Material coefficients were gathered from the literature, which does not take into accout subject-specific differences in structure and strength of the IGHL and cartilage. Insertion sites were assumed to be rigid, which does not account for deformation that occurs where the IGHL inserts into the humerus and scapula. This could have an effect on predicted stresses and strains in this area of the IGHL. Originally, it was thought that the fiber orientation in the IGHL was aligned with the long axis of the "ligaments," so a transversly isotropic hyperelastic material model [53] was used in a previous model of just the AB-IGHL. However, Debski et al. [32] demonstrated that, although there may be local fiber alignment in some regions of the capsule, there is no global material symmetry. Thus, an isotropic hypoelastic constitutive model was used to represent the IGHL.

The kinematics of the experiments that were examined in this study resulted in considerable distortion, bending and buckling of the IGHL. It is difficult to accurately represent the bending and buckling with low-order hexahedral elements, since these elements tend to be very stiff in bending and thus can easily "invert" during the Newton iterations, which leads to problems with convergence. This problem was alleviated by the use of shell elements as described in the Methods section above. Since shell elements are essentially two-dimensional (although the thickness is taken into account for stress and strain calculations), they will not invert due to deformation through the thickness and only in-plane deformations can cause inversion. They also have the added benefit of enhanced flexibility in bending and thus they provide a better representation of the physics of thin stuctures such as the glenohumeral capsule [44] [43].

Future studies will address some of the limitations and assumptions described above by modeling a larger portion of the capsule and by constructing multiple subject-specific finite element models, each with specific kinematics and possibly specific material properties. A robotic/universal force-moment sensor testing system will be utilized to determine the force distribution in each portion of the glenohumeral joint capsule [50]. These forces can then be used to validate the FE models. This procedure will be repeated for each subject-specific specimen for which a FE model is constructed. By using multiple FE models, the significance and relevance of results can be increased.

In summary, computational methods have been developed for study of the three-dimensional deformation of the IGHL during the simple translation test. A subject-specific FE modeling technique was used to predict experimental stress, strain and contact force measurements. The techniques developed and applied in this study are necessary to accurately predict the complex strain and stress patterns that occur in the shoulder joint capsule as it undergoes large deformation and wrapping around the cartilage and bone of the humerus. The methodologies developed in this research can be readily adapted to the study of other regions of the glenohumeral capsule and alternative loading schemes.

This research will provide a foundation for further studies of the capsulo-ligamentous soft tissue structures of the shoulder and patient-specific clinical treatment. Since the IGHL complex is the primary static stabilizer of the shoulder, precise understanding of its function not only will aid clinicians in diagnosis of shoulder instability but also will result in techniques for optimal repair procedures.

APPENDIX

This appendix demonstrates the method described by Simo and Qu-Voc to convert the transformation matrices from the tracking system into quaternions [37], and convert the quaternions for use in the finite element code. The commercially available program Matlab 6.1 (The Mathworks, Inc.) was used to execute the code. The transformation matrix between the registration blocks was obtained from the tracking system for each time step:

$$T = \begin{bmatrix} R_{11} & R_{12} & R_{13} & t_1 \\ R_{21} & R_{22} & R_{23} & t_2 \\ R_{31} & R_{32} & R_{33} & t_3 \\ 0 & 0 & 0 & 1 \end{bmatrix}. \tag{3.1}$$

Here the R_{ij} are the components of the 3x3 rotation matrix and the t_i are the components of the translation vector. Next, Spurrier's Algorithm was used to derive the quaternions corresponding to each transformation matrix:

```
%Compute the trace of the matrix.  Initialize the flag.
T = matrix(a+1:a+3,1:3);                                    (3.2)
trc = T(1,1) + T(2,2) + T(3,3);
M = trc;
flag = 0;

%Loop through the matrices to test a condition.
for i=1:3,
  if T(i,i) > M
    M = T(i,i);
    flag = i;
  end
end
```

```
%Compute the quaternions based on the value of the flag.
if flag == 0
  q(1) = 0.5*sqrt(1.0+trc);
  q(2) = (T(3,2) - T(2,3))/(4*q(1));
  q(3) = (T(1,3) - T(3,1))/(4*q(1));
  q(4) = (T(2,1) - T(1,2))/(4*q(1));
end

if flag == 1
  q(2) = sqrt(0.5*M + 0.25*(1-trc));
  q(1) = (T(3,2) - T(2,3))/(4*q(2));
  q(3) = (T(2,1) + T(1,2))/(4*q(2));
  q(4) = (T(3,1) + T(1,3))/(4*q(2));
end

if flag == 2
  q(3) = sqrt(0.5*M + 0.25*(1-trc));
  q(1) = (T(1,3) - T(3,1))/(4*q(3));
  q(4) = (T(3,2) + T(2,3))/(4*q(3));
  q(2) = (T(1,2) + T(2,1))/(4*q(3));
end

if flag == 3
  q(4) = sqrt(0.5*M + 0.25*(1-trc));
  q(1) = (T(2,1) - T(1,2))/(4*q(4));
  q(2) = (T(1,3) + T(3,1))/(4*q(4));
  q(3) = (T(2,3) + T(3,2))/(4*q(4));
end
```

Here, "trc" is the trace of the matrix, or $T_{11}+T_{22}+T_{33}$, where T is the transformation matrix and q is the quaternions. Then, the "load curves," or incremental translations and rotations used for input into the finite element code were extracted from the quaternions using a method outlined by Maker [38]:

```
%Alpha is a variable.  Calculate the magnitude of the last three quaternions.
alpha = (sqrt(q(2)*q(2) + q(3)*q(3) + q(4)*q(4)))                    (3.3)

if alpha < 0.000001
  beta = 0.0;
end
```

```
  if alpha >= 0.000001
     beta = (2/alpha) * asin(alpha);
   end

% rx, ry, and rz are the values for NIKE3D load curves
% These are stored in columns.
   rx(l,1) = beta*q(2);
   ry(l,1) = beta*q(3);
   rz(l,1) = beta*q(4);
   dx(l,1) = rztest(a+1,4);
   dy(l,1) = rztest(a+2,4);
   dz(l,1) = rztest(a+3,4);
end
```

Here, α is calculated from the quaternions, β is calculated from α and the incremental rotations (r_x, r_y and r_z) are calculated from both beta and the quaternions. The incremental translations (*dx*, *dy* and *dz*) come from the transformation matrix. The last step is to difference the incremental rotations and translations from the values of the previous time step and start the load curves at zero.

REFERENCES

[1] S. J. Turkel, M. W. Panio, J. L. Marshall, and F. G. Girgis, "Stabilizing mechanisms preventing anterior dislocation of the glenohumeral joint," *J Bone Joint Surg Am*, vol. 63, pp. 1208-17., 1981.

[2] A. S. B. Bankart, "Recurrent or habitual dislocation of the shoulder joint," *Br Med J*, vol. 2, pp. 1132-3, 1923.

[3] T. S. Atkinson, R. C. Haut, and N. J. Altiero, "A poroelastic model that predicts some phenomological responses of ligaments and tendons," *J Biomech Eng*, vol. 119, pp. 400-5, 1997.

[4] M. Z. Bendjaballah, A. Shirazi-Adl, and D. J. Zukor, "Finite element analysis of human knee joint in varus-valgus," *Clin Biomech*, vol. 12, pp. 139-48, 1997.

[5] J. C. Gardiner and J. A. Weiss, "Experimental testing and computational modeling to determine the stress-strain distribution in the human medial collateral ligament," *Trans 44th Annual ORS Meeting*, vol. 23, pp. 1027, 1998.

[6] J. H. Heegaard, P. F. Leyvraz, and A. Curnier, "The biomechanics of the human patella during passive knee flexion," *J Biomech*, vol. 28, pp. 1265-79, 1995.

[7] S. Hirokawa and R. Tsuruno, "Three-dimensional deformation and stress distribution in an analytical/computational model of the anterior cruciate ligament," *J Biomech*, vol. 33, pp. 1069-1077, 2000.

[8] A. F. DePalma, G. Callery, and G. A. Bennett, "Variational anatomy and degenerative lesions of the shoulder joint," *American Academy of Orthopaedic Surgery Instructional Course Lecture Series*, vol. 6, pp. 225-81, 1949.

[9] S. J. O'Brien, M. C. Neves, S. P. Arnoczky, S. R. Rozbruck, E. F. Dicarlo, R. F. Warren, R. E. Schwartz, and T. L. Wickiewicz, "The anatomy and histology of the inferior glenohumeral ligament complex of the shoulder," *Am J Sports Med*, vol. 18, pp. 449-56, 1990.

[10] J. Ovesen and S. Nielsen, "Stability of the shoulder joint. Cadaver study of stabilizing structures.," *Acta Orthop Scand*, vol. 56, pp. 149-51, 1985.

[11] J. M. Stefko, Tibone, J. E., Cawley, P. W., ElAttrache, N. E., McMahon, P. J., "Strain of the anterior band of the inferior glenohumeral ligament during capsule failure," *J Should Elbow Surg*, vol. 6, pp. 473-479, 1997.

[12] P. J. McMahon, Tibone, J. E., Cawley, P. W., Hamilton, C., Fechter, J. D., ElAttrache, N. S., Lee, T. Q., "The anterior band of the inferior glenohumeral ligament: Biomechanical properties from tensile testing in the position of apprehension," *J Should Elbow Surg*, vol. 7, pp. 467-471, 1998.

[13] L. U. Bigliani, Pollock, R. G., Soslowsky, L. J., Flatow, E. V., Pawluk, R. J., Mow, V. C., "Tensile Properties of the Inferior Glenohumeral Ligament," *J Orthop Res*, vol. 10, pp. 187-197, 1992.

[14] D. M. Malicky, L. J. Soslowsky, J. E. Kuhn, M. J. Bey, C. M. Mouro, J. A. Raz, and C. A. Liu, "Total strain fields of the antero-inferior shoulder capsule under subluxation: a stereoradiogrammetric study," *J Biomech Eng*, vol. 123, pp. 425-31., 2001.

[15] P. W. O'Connell, G. W. Nuber, R. A. Mileski, and E. Lautenschlager, "The contribution of the glenohumeral ligaments to anterior stability of the shoulder joint.," *Am J Sports Med*, vol. 18, pp. 579-84, 1990.

[16] S. L. Brenneke, J. Reid, R. P. Ching, and D. L. Wheeler, "Glenohumeral kinematics and capsulo-ligamentous strain resulting from laxity exams.," *Clin Biomech*, vol. 15, pp. 735-42, 2000.

[17] S. M. Moore, P. J. McMahon, and R. E. Debski, "Bi_Directional mechanical properties of the axillary pouch of the glenohumeral capsule: implications for modeling and surgical repair.," *J Biomech*, pp. In Revision, 2002.

[18] R. E. Schwartz, S. J. O'Brien, R. F. Warren, and P. A. Torzilli, "Capsular restraints to anterior-posterior motion of the abducted shoulder. A biomechanical study.," *Orthopaedic Transactions*, vol. 12, pp. 727, 1988.

[19] J. J. P. Warner, D. N. Caborn, R. Berger, F. H. Fu, and M. Seel, "Dynamic capsuloligamentous anatomy of the glenohumeral joint," *J Should Elbow Surg*, vol. 2, pp. 115-33, 1993.

[20] J. J. P. Warner, X. H. Deng, R. F. Warren, and P. A. Torzilli, "Static capsuloligamnetous restraints to superior-inferior translation of the glenohumeral joint," *Am J Sports Med*, vol. 20, pp. 675-85, 1992.

[21] N. D. Boardman, R. E. Debski, J. J. P. Warner, E. Taskiran, L. Maddox, A. B. Imhoff, F. H. Fu, and S. L.-Y. Woo, "Tensile properties of the superior glenohumeral and coracohumeral ligaments," *J Should Elbow Surg*, vol. 5, pp. 249-54, 1996.

[22] E. Itoi, J. J. Grabowski, B. F. Morrey, and K.-N. An, "Capsular properties of the shoulder," *Tohoku J Exp Med*, vol. 171, pp. 203-10, 1993.

[23] T. Q. Lee, J. Dettling, M. D. Sandusky, and P. J. McMahon, "Age related biomechanical properties of the glenoid-anterior band of the inferior glenohumeral ligament-humerus complex," *Clin Biomech (Bristol, Avon)*, vol. 14, pp. 471-6, 1999.

[24] P. J. McMahon, J. Dettling, M. D. Sandusky, J. E. Tibone, and T. Q. Lee, "The anterior band of the inferior glenohumeral ligament. Assessment of its permanent deformation and the anatomy of it's glenoid attachment," *J Bone Joint Surg Br*, vol. 81, pp. 406-13, 1999.

[25] J. B. Ticker, L. U. Bigliani, L. J. Soslowsky, R. J. Pawluk, E. L. Flatow, and V. C. Mow, "Inferior glenohumeral ligament: geometric and strain-rate dependant properties," *J Should Elbow Surg*, vol. 5, pp. 269-79, 1996.

[26] Z. P. Luo, H. C. Hsu, J. J. Grabowski, B. F. Morrey, and K.-N. An, "Mechanical environment associated with rotator cuff tears," *J Should Elbow Surg*, vol. 7, pp. 616-20, 1998.

[27] J. E. Novotny, B. D. Beynnon, and C. E. Nichols, "Modeling the stability of the human glenohumeral joint during external rotation," *J Biomech*, vol. 33, pp. 345-54, 2000.

[28] F. C. Van der Helm, "A finite element musculoskeletal model of the shoulder mechanism," *J Biomech*, vol. 27, pp. 551-69, 1994.

[29] F. C. Van der Helm, "Analysis of the kinematic and dynamic behavior of the shoulder mechanism," *J Biomech*, vol. 27, pp. 527-50, 1994.

[30] R. E. Debski, Wong, E. K., Woo, SL-Y, Fu, F.H., Warner, J.J.P., "An analytical approach to determine the in situ forces in the glenohumeral ligaments," *J Biomech Eng*, vol. 121, pp. 311-315, 1999.

[31] F. Gohlke, E. Bernhard, and F. Schmitz, "The pattern of collagen fiber bundles of the capsule of the glenohumeral joint.," *J Should Elbow Surg*, vol. 3, pp. 111-28, 1994.

[32] R. E. Debski, S. M. Moore, J. L. Mercer, M. S. Sacks, and P. J. McMahon, "The collagen fibers of the anteroinferior capsulolabrum have multi-axial orientation to resist shoulder dislocation," *J Should Elbow Surg*, vol. 12, pp. 247-52, 2003.

[33] E. D. Hiester, Sacks, M.S., "Optimal bovine pericardial tissue selection sites. I. Fiber architecture and tissue thickness measurements," *J Biomed Mat Res*, vol. 39, pp. 207-14, 1998.

[34] M. S. Sacks, Smith, D.B., Hiester, E.D., "A small angle light scattering device for planar connective tissue microstructural analysis," *Ann Biomed Eng*, vol. 25, pp. 678-89, 1997.

[35] K. J. Fischer, T. T. Manson, H. J. Pfaeffle, M. M. Tomaino, and S. L. Woo, "A method for measuring joint kinematics designed for accurate registration of kinematic data to models constructed from CT data," *J Biomech*, vol. 34, pp. 377-83., 2001.

[36] R. E. Debski, McMahon, P. J., Thompson, W.O., Warner, J.P.P., Woo, SL-Y, Fu, F. U., "A new dynamic testing apparatus to study glenohumeral joint motion," *J Biomech*, vol. 27, pp. 869-874, 1995.

[37] J. C. Simo, Vu-Quoc, L., "On the dynamics in space of rods undergoing large motions - a geometrically exact approach," *Comp Meth Appl Mech Eng*, vol. 66, pp. 125-161, 1988.

[38] B. N. Maker, "Rigid bodies for metal forming analysis with NIKE3D," *University of California, Lawrence Livermore Lab Report*, vol. UCRL-JC, pp. 1-8, 1995.

[39] D. M. Malicky, L. J. Soslowsky, C. M. Mouro, J. Frisancho, S. Lindholm, and J. E. Kuhn, "Total and nonrecoverable strain fields of the glenohumeral joint capsule under shoulder subluxation.," *Transcripts of the Orthopaedic Research Society*, vol. 40, pp. 94, 1999.

[40] J. D. Boissonnat, "Shape reconstruction from planar cross-sections," *Computer Vision, Graphics and Image Processing*, vol. 44, pp. 1-29, 1988.

[41] B. N. Maker, R. M. Ferencz, and J. O. Hallquist, "NIKE3D: A nonlinear, implicit, three-dimensional finite element code for solid and structural mechanics," *Lawrence Livermore National Laboratory Technical Report*, vol. UCRL-MA-105268, 1990.

[42] R. B. Little, H. W. Wevers, D. Siu, and T. D. Cooke, "A three-dimensional finite element analysis of the upper tibia," *J Biomech Eng*, vol. 108, pp. 111-9., 1986.

[43] T. J. R. Hughes and W. K. Liu, "Nonlinear finite element analysis of shells: Part I. Three dimensional shells," *Comp Meth Appl Mech Eng*, vol. 26, pp. 331-62, 1981.

[44] T. J. R. Hughes and E. Carnoy, "Nonlinear finite element shell formulation accounting for large membrane strains," *Comp Meth Appl Mech Eng*, vol. 39, pp. 69-82, 1983.

[45] H. Matthies and G. Strang, "The solution of nonlinear finite element equations," *Int J Numer Methods Eng*, vol. 14, pp. 1613-1626, 1979.

[46] W. J. Newman, R. E. Debski, J. C. Gardiner, S. M. Moore, and J. A. Weiss, "Function of the anterior band of the inferior glenohumeral ligament during the load and shift test," *ASME Adv Bioeng*, 2002.

[47] F. A. Matsen, Fu, F. H., Hawkins, R. J., *The Shoulder: A Balance of Mobility and Stability*. Rosemont, IL: American Academy of Orthopaedic Surgeons, 1992.

[48] J. C. Gardiner and J. A. Weiss, "Effects of flexion angle and valgus rotation on stresses in the human medial collateral ligament," *Proc ASME Bioeng Conf*, vol. BED-35, pp. 27-28, 1997.

[49] J. C. Gardiner, J. A. Weiss, and T. D. Rosenberg, "Strain in the human medial collateral ligament during valgus loading of the knee," *Clinical Orthopaedics and Related Research*, 2001.

[50] R. E. Debski, E. K. Wong, S. L.-Y. Woo, M. Sakane, F. H. Fu, and J. J. P. Warner, "In situ force distribution in the glenohumeral joint capsule during anterior-posterior loading," *J Orthop Res*, vol. 17, pp. 769-76, 1999.

[51] A. C. Burkart, R. E. Debski, V. Musahl, and P. J. McMahon, "Glenohumeral translations are only partially restored after repair of a simulated type II superior labral lesion.," *Am J Sports Med*, vol. 31, pp. 56-63, 2003.

[52] A. M. Halder, S. G. Kuhl, M. E. Zobitz, D. Larson, and K.-N. An, "Effects of the glenoid labrum and glenohumeral abduction on stability of the shoulder joint through concavity-compression," *J Bone Joint Surg*, vol. 83-A, pp. 1062-9, 2001.

[53] J. A. Weiss, B. N. Maker, and S. Govindjee, "Finite element implementation of incompressible, transversely isotropic hyperelasticity," *Computer Methods in Applied Mechanics and Engineering*, vol. 135, pp. 107-128, 1996.